UC Davis

UC Davis Previously Published Works

Title

Predictions and Validations of Small-Scale Rotor Noise Using UCD-QuietFly

Permalink

https://escholarship.org/uc/item/8947p9rc

Journal

Aeromechanics for Advanced Vertical Flight Technical Meeting 2022

Authors

Li, S

Lee, S

Publication Date

2022

eScholarship.org Powered by the California Digital Library
University of California

Predictions and Validations of Small-Scale Rotor Noise Using UCD-QuietFly

Sicheng (Kevin) Li
Ph.D. Candidate

Seongkyu Lee
Associate Professor

Department of Mechanical and Aerospace Engineering
University of California, Davis
Davis, California, 95616 U.S.A.

ABSTRACT

A physics-based broadband noise prediction approach is applied for small-scale drone rotors that have small chord lengths, low Reynolds numbers, and high rotational speeds. These unique characteristics, different from conventional full-scale rotors, are studied in the improved noise prediction models presented in this paper. The Roger and Moreau's trailing-edge boundary condition and leading-edge back-scattering correction are included in the Amiet's trailing-edge noise model in UCD-QuietFly. An incident field correction is proposed in this paper to account for the modified trailing-edge boundary condition. The laminar boundary layer-vortex shedding (LBL-VS) noise prediction is implemented in UCD-QuietFly using the semi-empirical Brooks-Pope-Marcolini (BPM) model. The theoretical predictions are validated against the experiments on three small-scale drone rotors in hovering and forward flights. LBL-VS noise is found to be an important noise source for untripped blades, but the BPM model requires an ad hoc tuning for good predictions. The effect of leading-edge back-scattering in broadband noise is found to be important for small-scale rotors at low frequencies when the reduced frequency (kc) is below 1.17. Finally, broadband noise is compared for different blade designs. At the same thrust, the ideally twisted rotor generates slightly higher broadband noise than the linearly twisted rotor, while the tapered blade tip is shown to reduce the broadband noise levels significantly.

NOTATION

c	chord length, m
c_0	speed of sound, m/s
C_T	rotor thrust coefficient
C_P	rotor power coefficient
E^*	complex conjugate of a Fresnel integral
FM	figure of merit
f	frequency, Hz
k	acoustic wavenumber, ω/c_0
K	aerodynamic wavenumber, ω/V
$\bar{K}_x$	normalized streamwise wavenumber, $\omega c/2V_c$
L	effective lift function, N/m
l_y	spanwise turbulence lengthscale, $1.6V_c/\omega$, m
M	blade sectional flow Mach number
M_∞	rotor forward Mach number
N_b	number of blades
OASPL	overall sound pressure level, dB
R	rotor radius, m
R_c	chord Reynolds number
RPM	round per minute
r	blade radial location, m
S_{pp}	acoustic PSD, Pa^2/Hz
SPL	sound pressure level, dB
St	Strouhal number, $f\delta_p/V$
V	blade sectional freestream velocity, m/s
V_c	convection velocity, $0.7V$, m/s
V_i	induced velocity, m/s
X,Y,Z	observer global coordinates, m
$\vec{x}$	observer position, m
α^*	effective angle of attack, deg
α_{sh}	rotor shaft angle of attack, deg
δ^*	boundary layer displacement thickness, m
δ_p	pressure side boundary layer thickness, m
Δr	blade section span, m
ω	angular frequency, rad/s
Φ_{pp}	surface pressure spectrum, Pa^2/Hz
ϕ_o	observer elevation angle, deg
σ	rotor solidity
θ_{tw}	blade linear twist rate, deg
θ_0	collective pitch angle, deg

Presented at the 2022 VFS Aeromechanics for Advanced Vertical Flight Technical Meeting, San Jose, California, USA, January 25-27, 2022.

INTRODUCTION

In recent years, the industry of small unmanned aircraft systems (sUAS) or drones has rapidly emerged for both civil and defense applications (Refs. 1,2,3). Powered by small-scale rotors, these aircraft are widely used for logistics, surveillance, and recreation. However, noise is one of the top barriers to the wider deployment of the UAS aircraft, which involves different noise characteristics from full-scale helicopter rotors.

For conventional helicopters, tonal noise, occurring at discrete frequencies in the low-frequency range, is the dominant

noise source in the forward and rearward directions (Ref. 4), while broadband noise is important in the downward direction (Ref. 5). The strong tonal noise results from the aerodynamic characteristics of conventional helicopters. For instance, a transonic rotor blade tip generates high-speed impulsive noise propagating in the forward direction (Ref. 6). Strong tip vortices are formed to create blade-vortex-interaction (BVI) noise that is dominant for multi-rotors (Refs. 7,8,9,10). The variation of blade loading creates unsteady loading noise at high forward speed. Thickness noise is also important for high-speed rotor blades. Regarding broadband noise on full-scale rotors, fully turbulent boundary layer flows occur in the rotor tip regions at high Reynolds number (Ref. 11). Therefore, turbulent boundary layer flow trailing-edge noise is the dominant broadband noise source in hovering and forward flights, while blade-wake-interaction (BWI) noise is a vital broadband noise source in descending flight (Ref. 12).

On the contrary, small-scale rotors have different noise characteristics from conventional helicopters, due to their low tip speeds and small blade sizes. Experiments have shown that the importance of tonal noise is reduced while the broadband noise becomes more critical on small-scale rotors (Ref. 13). In addition, the A-weighted sound pressure level (SPL) shows that the broadband noise is more important on drone rotors at high frequencies considering human perception (Ref. 14). The reduced rotor tip speed considerably lowers the tonal noise strength, while the tip speed reduction has weaker effects on broadband noise (Ref. 15). For example, on a mid-scale BO-105 rotor (Ref. 12) with the rotor radius of 2 m and the tip Mach number of 0.32, the tip Reynolds number is 1 million; however, on a small drone rotor (Ref. 16) with the rotor radius of 0.16 m and the tip Mach number of 0.15, its tip Reynolds number is about 0.1 million. It is seen that the fully turbulent boundary layer flow can be developed in the tip regions of the BO-105 rotor, while the drone rotor can have a laminar boundary layer on the entire blade, where vortex-shedding noise becomes a critical broadband noise source. In addition, due to the short chord length of the small-scale rotors, the effect of leading-edge back-scattering can be important with the small reduced frequency kc (Ref. 17). Thus, the broadband noise prediction methods specialized for small-scale rotors must be developed and validated.

Turbulent boundary layer trailing-edge (TBL-TE) noise (Ref. 18) is still one of the most important broadband noise sources for small-scale rotors. Amiet's trailing-edge noise model (Ref. 19) was developed to predict this trailing-edge noise based on Curle's acoustics analogy (Ref. 20) in conjunction with Schwartzchild's solution (Ref. 21) for acoustic scattering. Amiet's original model only included the trailing-edge scattering, but the leading-edge back-scattering and the sub-critical gusts were incorporated later in Roger and Moreau's model (Ref. 17). The improved trailing-edge boundary condition for Amiet's model was proposed based on new interpretations of the Kutta condition (Ref. 22). While the original Amiet model (Ref. 23) supposed that the pressure around the trailing edge on each side of the wake is equal to half of the incident pressure, the modified Roger and Moreau's theory (Ref. 17) suggested that the wake pressure on both the upper and lower sides of the wake should be zero. Although both theories satisfied the Kutta condition as the pressure difference between the upper and lower sides is zero, the larger eddy simulation (LES) (Ref. 24) indicated that the latter was closer to the flow physics. The strengths of these physics-based models, such as Amiet's model (Ref. 19) or Howe's model (Ref. 25), have been demonstrated by their capabilities to investigate the noise reduction techniques, including the trailing-edge serrations (Refs. 26,27) and the swept blades (Ref. 28). Regarding the rotorcraft applications, Amiet's model was recently used to study broadband noise of urban air mobility (UAM) vehicles (Ref. 29).

The prediction methods of small-scale rotors have been explored through different approaches. First, Lattice-Boltzmann Method / Very Large Eddy Simulation (LBM/VLES) was used to capture the boundary layer transition and laminar separation bubble accurately. LBM/VLES method was also used to predict the BWI noise of a small rotor in hover (Ref. 30). Broadband noise was obtained using the Ffowcs-Williams and Hawkings (FW-H) equation and validated on a low Reynolds number propeller (Ref. 31). Regarding tonal noise, the low-fidelity tools, such as the BEMT/FW-H method, were proved to provide accurate results for small-scale rotors (Ref. 31). Second, broadband noise of a small ideally twisted rotor was predicted using the NASA Aircraft Noise Prediction Program (ANOPP), which was based on the semi-empirical Brooks-Pope-Marcolini (BPM) model developed based on NACA0012 airfoil (Refs. 16,32). Third, broadband noise of a drone rotor with the tripped boundary layer was predicted using a physics-based tool, UCD-QuietFly (Ref. 11), which used Amiet's trailing-edge noise model (Ref. 19) and Lee's wall pressure spectrum model (Ref. 33). High-fidelity computational fluid dynamics (CFD) was coupled with UCD-QuietFly to predict broadband noise on an APC drone rotor (Ref. 34). UCD-QuietFly was shown to be a feasible method to predict small-scale rotors, but improvement needs were identified for more consistent predictions in small-scale rotors (Ref. 35).

In this paper, an improved approach to predict broadband noise of small-scale rotors is presented using the rotor-broadband noise prediction tool UCD-QuietFly (Ref. 29). The effects of leading-edge back-scattering, the importance of laminar-boundary-layer vortex-shedding (LBL-VS) noise, and an improved Amiet's model are studied. The new method is validated against various small-scale rotor experiments. Finally, the effects of rotor blade twist and taper on broadband noise are investigated.

METHOD AND FORMULATION

Roger and Moreau's trailing-edge noise model (Ref. 17) reads

$$S_{pp}(\vec{x},\omega) = \left(\frac{kcZ}{4\pi S_0^2}\right)^2 2\Delta r|\mathbf{L}|^2\Phi_{pp}(\omega)l_y(\omega) \qquad (1)$$

where $S_0^2 = X^2 + \beta^2\left(Y^2+Z^2\right)$, $\beta^2 = 1-M^2$, k is the acoustic wavenumber, c is the chord length, Δr is the blade sec-

tional span, L is the loading term, l_y is the spanwise turbulence correction length, and Φ_{pp} is the wall pressure spectrum (Ref. 33). The X,Y,Z coordinates are shown in Fig. 1

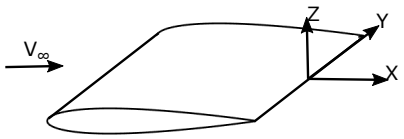

Fig. 1: Blade section local coordinate

Note that Eq. (1) is four times in magnitude of the original Amiet model (Refs. 19,36). While the original Amiet model assumes the zero pressure jump at the trailing edge, Roger and Moreau (Ref. 22) assumed zero pressure, which makes the scattered pressure twice of the incident pressure. As a different explanation, the scattering from one surface influences both the upper and lower surfaces. The remaining factor of two comes from the expected value of the complex conjugates. This updated trailing-edge noise model raises the noise levels by 6 dB and was shown to provide improved agreement with experiments (Ref. 37).

The loading term L includes the contributions from the trailing-edge scattering L_1 and the leading-edge back-scattering L_2, such that $L = L_1 + L_2$. In Roger and Moreau's formulations (Refs. 17,22), the entire trailing-edge scattering term L_1 was multiplied by a factor of four, including the incident field and the scattered field. However, the incident field should not be affected by the factor of four since the incident field is not affected by the trailing edge boundary condition or the Kutta condition. Thus, we propose a slight modification in Eq. (2), where the last term accounts for the incident field.

$$L_1 = -\frac{e^{2iC}}{iC}\left\{(1+i)e^{-2iC}\sqrt{\frac{B}{B-C}}E^*[2(B-C)] - (1+i)E^*[2B] + 1 - e^{-2iC} + \frac{e^{-2iC}}{4}\right\} \tag{2}$$

$$B = \bar{K}_x + M\bar{\mu} + \bar{\kappa} \tag{3}$$

$$C = \bar{K}_x - \bar{\mu}(X/S_0 - M) \tag{4}$$

Small-scale rotors have small chord lengths that result in the small reduced wavenumber kc, where the leading-edge back-scattering L_2 can be important at low frequencies. The Roger and Moreau's leading-edge back-scattering correction (Ref. 17) reads

$$\frac{1}{H}L_2 = \left\{e^{4i\bar{\kappa}}[1-(1+i)E^*(4\bar{\kappa})]\right\}^c - e^{2iD} + i[D + k_x^* + M\bar{\mu} - \bar{\kappa}]G \tag{5}$$

where

$$H = \frac{(1+i)e^{-4i\bar{\kappa}}(i-\Theta^2)}{2\sqrt{\pi}(\alpha-1)k_x^*\sqrt{B}} \tag{6}$$

$$D = \bar{\kappa} - \bar{\mu}X/S_0; \quad \alpha = V/V_c \tag{7}$$

$$\Theta = \sqrt{\frac{\bar{K}_x + \bar{\mu}M + \bar{\kappa}}{k_x^* + \bar{\mu}M + \bar{\kappa}}} \tag{8}$$

$$G = (1+\varepsilon)e^{i(2\bar{\kappa}+D)}\frac{\sin D - 2\bar{\kappa}}{D-2\bar{\kappa}} + (1-\varepsilon)e^{i(-2\bar{\kappa}+D)}\frac{\sin D + 2\bar{\kappa}}{D+2\bar{\kappa}} + \frac{(1+\varepsilon)(1-i)}{2(D-2\bar{\kappa})}e^{4i\bar{\kappa}}E^*(4\bar{\kappa}) - \frac{(1-\varepsilon)(1+i)}{2(D+2\bar{\kappa})}e^{-4i\bar{\kappa}}E^*(4\bar{\kappa}) + \frac{e^{2iD}}{2}\sqrt{\frac{2\bar{\kappa}}{D}}E^*(2D)\left[\frac{(1+i)(1-\varepsilon)}{D+2\bar{\kappa}} - \frac{(1-i)(1+\varepsilon)}{D-2\bar{\kappa}}\right] \tag{9}$$

and the imaginary part of $\{\}^c$ in Eq. (5) is multiplied by $\varepsilon = (\sqrt{1+1/(4\bar{\mu})})^{-1}$.

The LBL-VS equations in the BPM model (Ref. 38) are implemented in UCD-QuietFly to predict vortex-shedding noise for low-Reynolds number conditions. The one-third-octave-band sound pressure level ($\mathrm{SPL}_{1/3}$) is explicitly calculated in Eq. (10), where G_1, G_2, and G_3 are empirically determined functions of Strouhal number, Reynolds number, and angle of attack. $\bar{D}_h$ is the directivity function in the BPM airfoil-self noise models.

$$\mathrm{SPL}_{LBL-VS} = 10\log\left(\frac{\delta_p M^5 \Delta r \bar{D}_h}{r_o^2}\right) + G_1\left(\frac{St'}{St'_{peak}}\right) + G_2\left[\frac{R_c}{(R_c)_0}\right] + G_3(\alpha^*) \tag{10}$$

RESULTS

This section presents the validations of the modified rotor broadband noise models. First, the predictions are validated on an airfoil in a 2-dimensional flow. Then, various small-scale rotors are used to validate UCD-QuietFly in both hovering and forward flights. Finally, the effects of the blade twist and taper on rotor broadband noise are presented.

A. Airfoil Validation

The modified model of airfoil trailing-edge noise is first validated against the airfoil-self noise experiments (Ref. 39) shown in Fig. 2. The tested blade section has a NACA0012 airfoil, with a chord length of 0.61 m, a span of 0.46 m, an observer distance of 1.2 m, and an observer angle of 90° directly above the airfoil section. The predictions agree well with the experiments for the entire frequency range, and the effect of flow speed is captured. It is seen that the modified

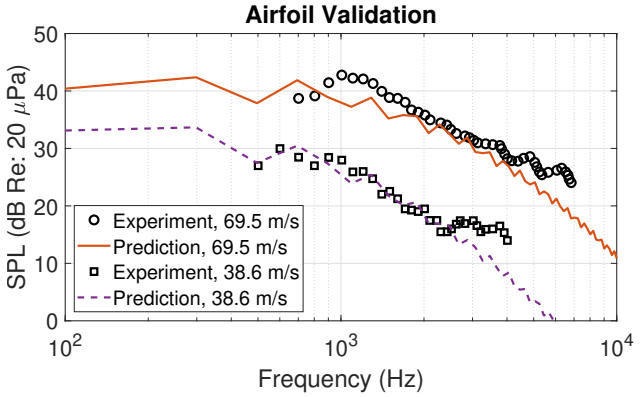

Fig. 2: Predictions of airfoil trailing-edge noise using the current model compared to the experimental data in Ref. 39 on a NACA0012 airfoil section, with chord length = 0.61 m, span = 0.46 m, observer distance = 1.2 m, and observer angle = 90°.

scattering factor (Ref. 17) and the corrected incident field suggested in this paper give excellent trailing-edge noise predictions on various flow speeds. With the modified theories validated in this 2-dimensional flow case, the following sections will present the validations of broadband noise predictions on various small-scale rotors in hovering and forward flight conditions.

B. Validations in Hovering Flight

Three different drone rotors are studied in UCD-QuietFly for their broadband noise. Table 1 shows the parameters and operating conditions of NASA ideally twisted rotor, SUI Endurance rotor, and DJI-CF rotor. The tip Mach number and Reynolds number are also given in Table 1, where all the rotor cases have the Reynolds numbers under 2×10^5. Although these low Reynolds numbers suggest that laminar flows occur on the entire blade span, the rotation-induced Coriolis force (Ref. 40) and the wake generated by the previous blade (Ref. 30) can destabilize the boundary layers to transit to turbulent flows. However, instead of investigating the case-dependent flow transitions on the individual rotors, the research interest of this paper is to explore a low-fidelity broadband noise method that can be practically generalized on small-scale rotors.

As the inputs to UCD-QuietFly, the blade radial distributions of the angle of attack and flow velocity are calculated in the blade element momentum theory (BEMT). For the ideally twisted rotor, the angle of attack and induced velocity distributions are shown in Fig. 3. It is seen that the induced velocity remains approximately unchanged in the radial direction except for the blade tip due to the ideal twist, which is desired to yield the minimum induced power. The angle of attack decreases at the hub and tip regions due to the tip loss effect. The broadband noise predictions of an ideally twisted small-scale rotor are shown in Figs 4 and 5 for two different rotational speeds on rough blades and smooth blades. The broadband noise components are shown in the

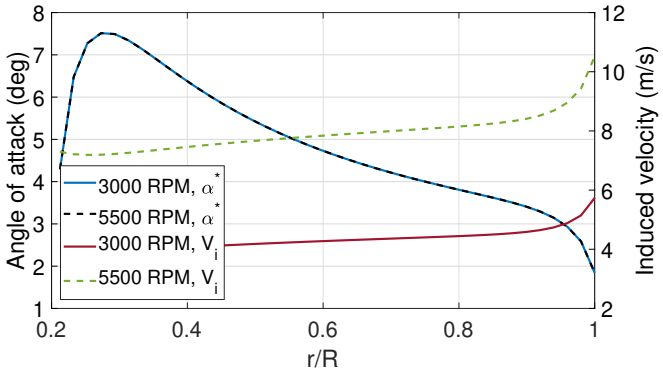

Fig. 3: Predictions of angle of attack and induced velocity from the blade element momentum theory (BEMT) on the ideally twisted rotor.

noise spectrum, including trailing-edge (TE) noise, vortex-shedding (VS) noise, trailing-edge bluntness (BL) noise, and airfoil-stall (ST) noise. The measurements were taken in the Small Hover Anechoic Chamber (SHAC) at the NASA Langley Research Center (Ref. 16).

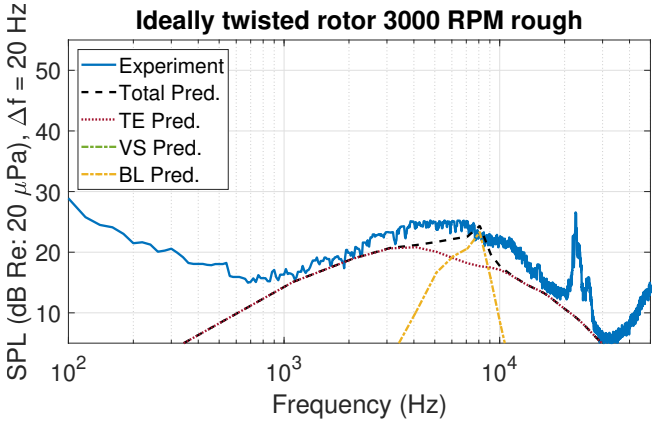

(a)

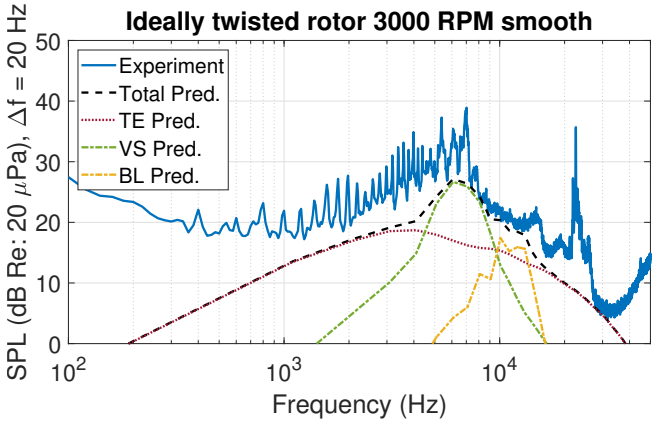

(b)

Fig. 4: Broadband noise predictions of the ideally twisted small rotor at 3000 RPM using UCD-QuietFly for: (a) rough blade surface, and (b) smooth blade surface. The experiment data is given in Ref. 16.

For the 3000 RPM case in Fig. 4, the predictions have excel-

Table 1: Parameters of small-scale rotors

Parameters	NASA ideally twisted rotor	SUI Endurance	DJI-CF
R (m)	0.1588	0.1904	0.12
σ (m)	0.255	0.0712	0.07
N_b	4	2	2
RPM	3000/5500	4800	4800/5400/6000
Tip M	0.1467/0.2690	0.2815	0.1774/0.1996/0.2218
Tip R_c (10^5)	1.0719/1.9652	0.7227	0.4244/0.4775/0.5305
C_T	0.0137	0.01	0.009
Airfoil	NACA0012	SUI	DJI-CF
r_o (m)	2.27	5.507	1.905
ϕ_o (deg)	-35	-40	-45

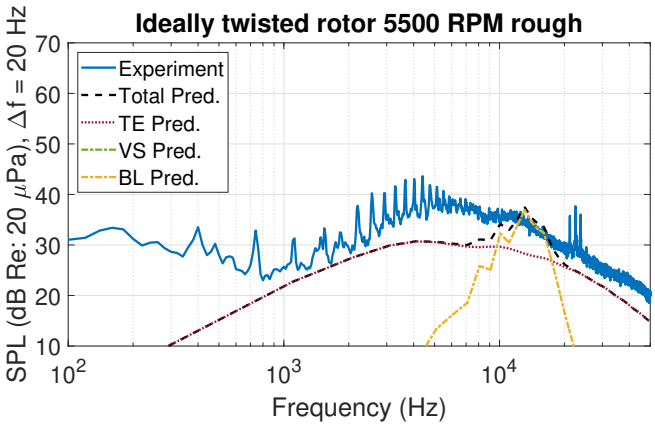

(a)

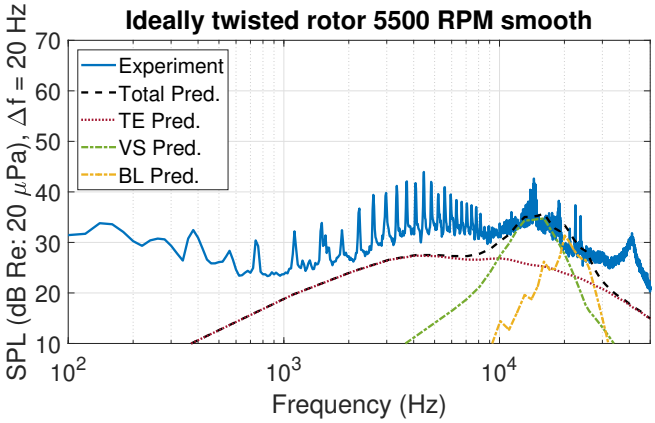

(b)

Fig. 5: Broadband noise predictions of the ideally twisted small rotor at 5500 RPM using UCD-QuietFly for: (a) rough blade surface, and (b) smooth blade surface. LBL-VS noise model is limited to $R_c < 1.8 \times 10^5$. The experiment data is given in Ref. 16.

lent agreement with the experiments above 1 kHz, in which the broadband noise sources are dominant. The rough blade has a fully turbulent flow, which is well captured by the TBL-TE noise. The smooth blade induces an LBL-VS noise peak at 7 kHz that is captured by the LBL-VS noise model in Eq. (10). In a higher rotational speed of 5500 RPM, the UCD-QuietFly under-predicts noise levels. However, the predictions well capture the noise increases in the entire frequency range for both the rough and the smooth blades with higher RPM. The 3000 RPM rotor has a higher noise level on the smooth blade, while the 5500 RPM rotor has a higher noise level on the rough blade. This trend is also predicted in UCD-QuietFly. Note that the LBL-VS noise model in Fig. 5(b) is manually limited for Reynolds number under 1.8×10^5, lower than the tip R_c in Table 1, to give the best prediction of LBL-VS noise level. Although this ad hoc method is impractical when measured data is not available, it is physically reasonable because flows near rotor tip regions can transit to turbulent flows at low Reynolds numbers due to Coriolis and wake effects (Refs. 40,30). The discrepancies between the predictions and the experiments for the ideally twisted rotor may come from the noise sources not included in our method, including blade-wake-interaction noise (broadband component below 0.6 kHz), motor noise, and tonal noise (discrete-frequency peaks).

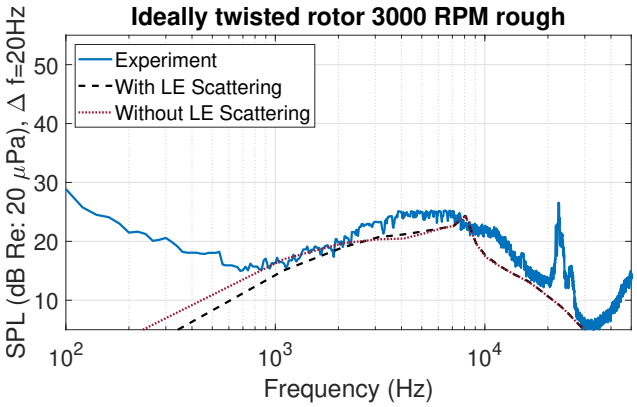

Fig. 6: Comparisons of the effects of the leading-edge back-scattering correction. The experiment data and BPM predictions are given in Ref. 32.

The effects of the leading-edge (LE) back-scattering correction are shown in Fig. 6 on the ideally twisted rotor with a rough surface and 3000 RPM. It is seen that including the leading-edge scattering gives about a 3 dB difference in the predictions at the low frequencies. The leading-edge scattering effect becomes important for the frequencies below 2 kHz,

corresponding to the reduced frequency of $kc = 1.17$.

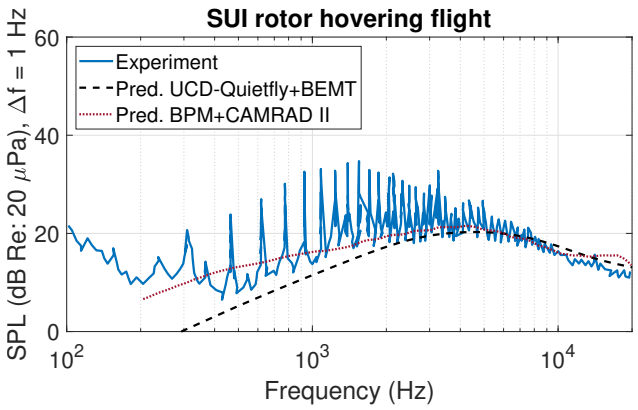

Fig. 7: Broadband noise predictions of the SUI Endurance rotor using UCD-QuietFly. The experiment data and BPM predictions are given in Ref. 32.

Broadband noise predictions and experimental data of SUI Endurance rotor in hovering flight are shown in Fig. 7. The acoustic experiment was conducted in the NASA Langley Low Speed Aeroacoustic Wind Tunnel (LSAWT)(Ref. 32), and the BPM model (Ref. 38) was used with CAMRAD II (Ref. 41) to obtain the BPM predictions (Ref. 32). The UCD-QuietFly predictions are obtained using the models presented in this paper, with the aerodynamics predicted in the BEMT. It is seen that UCD-Quietfly gives excellent broadband noise predictions for the entire frequency range, and the peak-level frequency is captured. Note that the broadband noise in the experiments is considered to be the bottom of the data where the effect of tonal noise is removed. In other words, our predictions are targeted to reach the bottom of the test data. Although the BPM prediction shows good overall agreement with the experiment, it gives about 5 dB overpredictions (above the bottom of the data) in the frequency range below 1 kHz. Note that in the BPM model, the acoustic results are empirically tuned based on NACA 0012 experiments, while UCD-Quietfly was developed based on the wall pressure spectrum modeling and physics-based acoustic scattering process. The SUI rotor uses cambered airfoils. Therefore, the discrepancies between the BPM and UCD-QuietFly predictions are possibly due to the airfoil effects, where a different airfoil profile can significantly change the boundary layer parameters near the airfoil trailing edge (Ref. 40).

Figure 8 shows the broadband noise validations of the DJI rotor in three rotational speeds. The angle of attack and the flow speed at each blade section are calculated using the BEMT, and the broadband noise components are predicted in UCD-QuietFly. The experimental data were measured in the Structural Acoustic Loads and Transmission (SALT) anechoic chamber facility at the NASA Langley Research Center (Ref. 13). The noise peaks levels are captured by the trailing-edge bluntness noise predictions. The predictions show good agreement with the experiments at 6000 RPM, but worse agreements at 4800 RPM and 5400 RPM. The predicted noise level increases with increasing rotational speed. However, the

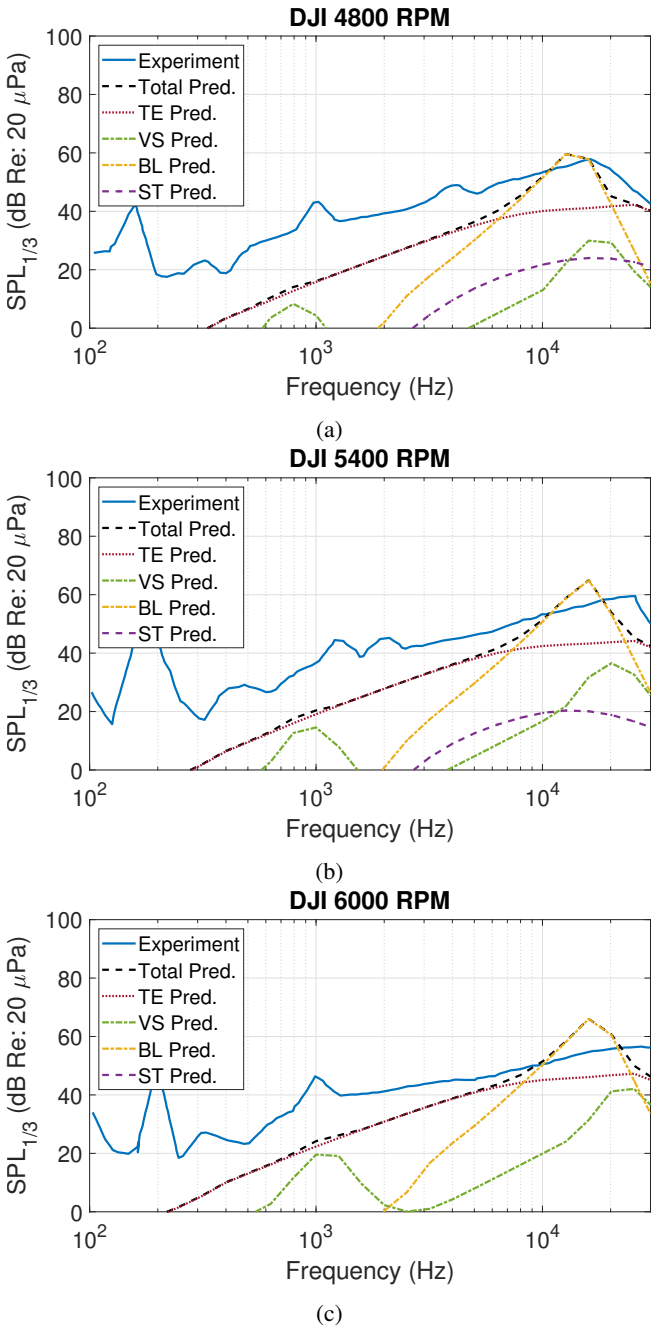

Fig. 8: Broadband noise predictions of the DJI-CF rotor using UCD-QuietFly at the rotational speeds of (a) 4800 RPM, (b) 5400 RPM, and (c) 6000 RPM. The experiment data is given in Ref. 13.

broadband components of the measured data remain the same at different RPMs, which might be due to the aeroelastic deflections of the rotor blades (Ref. 13). Therefore, the comparisons between the predictions and the experiments at different RPMs suggest that aeroelastic effects can be important in rotor broadband noise predictions and should be investigated in the future.

C. Validations in Forward Flight

This section presents the validations of rotor broadband noise predictions on a small-scale SUI Endurance rotor in forward flight. The rotor parameters are shown in Table 1, with rotor forward Mach number of 0.045 and shaft angle of attack of -10°. The SUI rotor forward flight analysis is carried out using an in-house BET code (Refs. 15,42), which includes the Peters-He dynamic inflow model (Ref. 43), the moment-balance trim solution (Ref. 44), and the blade element theory (BET). The predicted angle of attack distribution on the rotor disc is given in Fig. 9(a), and Fig. 9(b) shows the results from CAMRAD II (Ref. 32). It is seen that the in-house BET code agrees well with CAMRAD II, especially in the rotor tip regions that are acoustically important. The regions of high angles of attack are well predicted in the first quadrant and near 270° azimuthal angle.

The acoustic measurements of an isolated SUI single rotor in forward flight are shown in Fig. 10, which is given in Ref. 32. The predicted angle of attack and flow velocity at each blade section and each azimuthal angle are used in UCD-QuietFly to obtain the noise spectrum shown in Fig. 10, where time-averaging is taken in one rotor revolution. It is seen that the current models give excellent predictions in the frequency range (2-15 kHz) dominated by the airfoil-self noise sources, which covers the most sensitive range of human hearing (2-5 kHz).

D. Effects of Blade Twist and Taper

The effects of the blade twist and taper on rotor broadband noise are investigated, where the baseline case is the 5500 RPM ideally twisted rotor with the rough surface shown in Table 1. The baseline case has an ideal twist and a constant chord length. The parameters and performance coefficients of the three rotor cases are given in Table 2. The second rotor case has the same parameters as the baseline, except it has a linear twist of -10°. The third rotor case has a linear twisted of -10° and a 0.75 taper starting at 0.9 r/R. The collective pitch angle of the three rotor cases is adjusted to maintain the constant thrust coefficient. The radial distributions of the blade section pitch angle are shown in Fig. 11 for the three rotor cases. The performance data are calculated using the BEMT, where the linearly twisted rotor has a lower figure of merit than the ideally twisted rotor, and the tapered rotor has a higher figure of merit than the non-tapered rotors. Therefore, the designs of ideal twist and taper provide better performance. The three rotors have the same RPM in hovering conditions, and the observer is at -35° elevation angle and 2.27 m from the rotor hub.

The broadband noise predictions from UCD-QuietFly are shown in Fig. 12, and the overall sound pressure levels (OASPLs) of the three rotors are given in Table 2. The ideally twisted rotor has the highest noise level, and the linearly twisted and tapered rotor has the lowest noise level. As shown in Fig. 12(a), the noise differences among the three rotors are primarily in the frequency range covered by LBL-VS noise

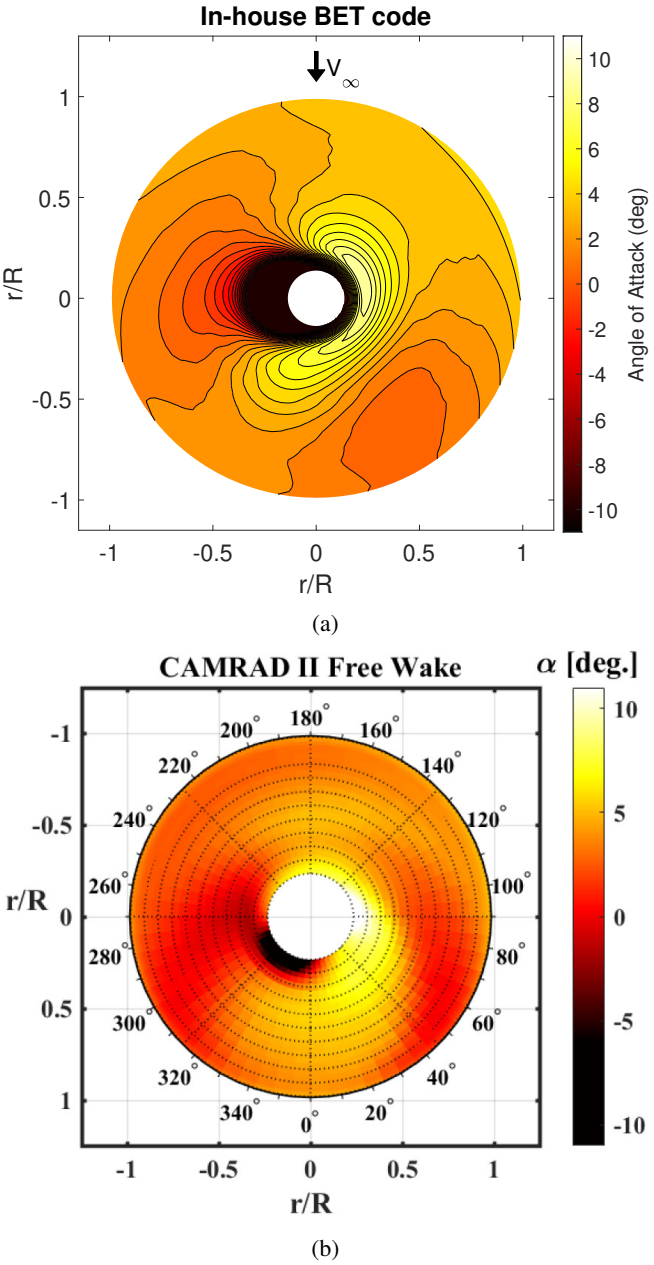

Fig. 9: Predictions of the SUI rotor forward flight angle of attack distribution at $\alpha_{sh} = -10°$ and $M_\infty = 0.045$ using: (a) in-house BET code, and (b) CAMRAD II (Ref. 32).

(15 kHz). Figure 12(b) shows the sectional contributions of OASPL. Although the root sections of the ideally twisted rotor generate lower noise than the other two cases, its tip sections give higher noise levels. As seen in Fig. 13(b), the radial distribution of the boundary layer displacement thickness on the pressure side indicates that the ideally twisted rotor has the highest δ^* at the tip region due to higher angles of attack. This thicker pressure side boundary thickness explains the higher LBL-VS noise on the ideally twisted rotor according to Eq. (10), where the suction side boundary layer thickness is not used. The tapered rotor generates lower LBL-VS noise due to its small chord length and small pressure side boundary layer thickness at the blade tip regions. Figure 12(b) shows that the

Table 2: Parameters of twisted and tapered rotors

Rotor case	θ_{tw}	θ_0	taper loc.	taper ratio	RPM	C_T	FM	C_P	OASPL
Ideal twist + const. chord	Ideal	34.5	No	No	5500	1.37E-2	0.649	1.75E-3	69.78
Linear twist + const. chord	-10	19.09	No	No	5500	1.37E-2	0.640	1.77E-3	68.25
Linear twist + tip taper	-10	19.17	0.9 r/R	0.75	5500	1.37E-2	0.467	1.75E-3	64.82

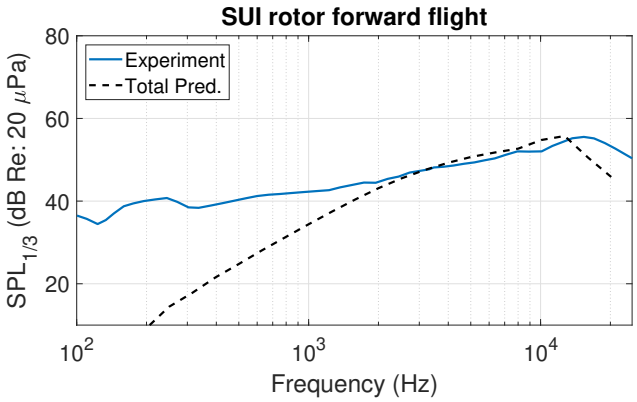

Fig. 10: Broadband noise predictions of the SUI rotor in forward flight using UCD-QuietFly. $\alpha_{sh} = -10^\circ$, $M_\infty = 0.045$, $\phi_o = -90$, $r_o = 3.54$ m. The experiment data is given in Ref. 32.

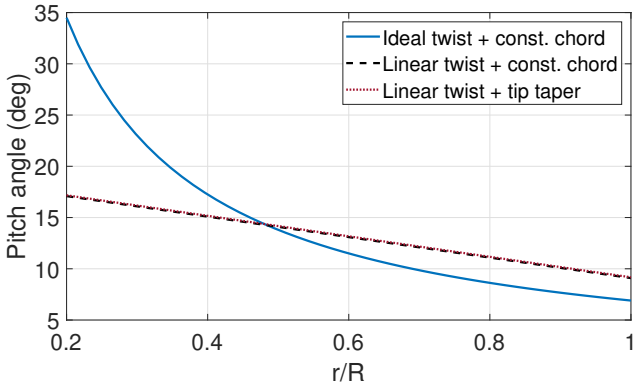

Fig. 11: Spanwise distributions of pitch angle for the three rotor cases.

ideally twisted rotor generates lower noise at the inboard regions, but its boundary layer displacement thickness on the suction side is large at the inboard regions. Although larger boundary layer displacement contributes to larger trailing-edge noise, the ideally twisted rotor has the large blade section pitch angle at the inboard regions, which results in its lower inboard sectional OASPL due to the directivity effect (away from the dipole directivity direction). Therefore, the effect of the ideal twist gives a slight increase of 1.53 dB in broadband noise level. On the other hand, the tip taper significantly reduced the broadband noise level by 3.43 dB.

CONCLUSIONS

This paper presents an improved prediction method for small-scale rotor broadband noise. The Amiet trailing-edge noise model in UCD-QuietFly is improved using Roger and

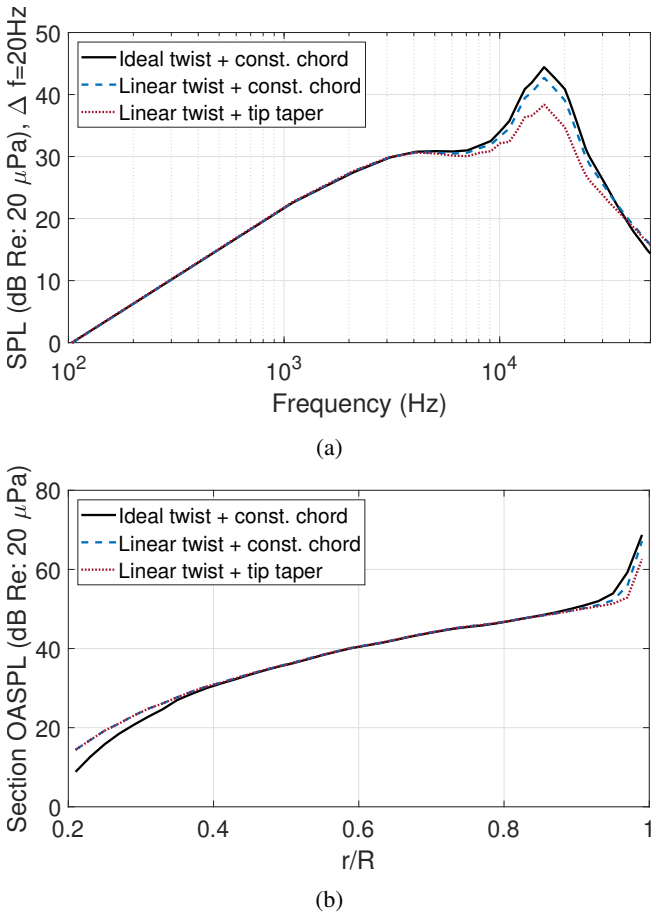

Fig. 12: Comparisons of the acoustic effects of the blade ideal twist, linear twist, and taper on the rotor at a constant thrust: (b) sound pressure level (SPL) spectrum, and (c) overall sound pressure level (OASPL) contributions of the radial sections.

Moreau's corrections of the leading-edge back-scattering and of the boundary condition at the trailing edge. A modified incident filed term is also proposed in this paper. Key findings are concluded as follows:

- Extensive validations of the current models were performed on NASA ideally twisted rotor, SUI Endurance rotor, and DJI-CF rotor. Various rotational speeds and surface roughness conditions were considered in the hovering flight and forward flight. The predictions from UCD-QuietFly agree well with the experiments in various small-scale rotor conditions.
- Laminar boundary layer-vortex shedding (LBL-VS) noise is shown to be an important broadband noise source for untripped small-scale rotors. The current LBL-VS

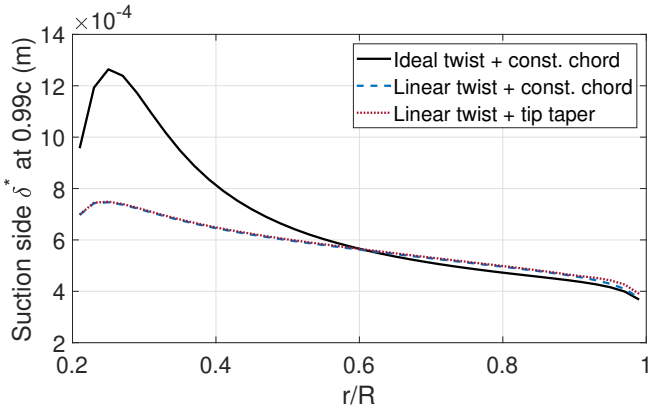

(a)

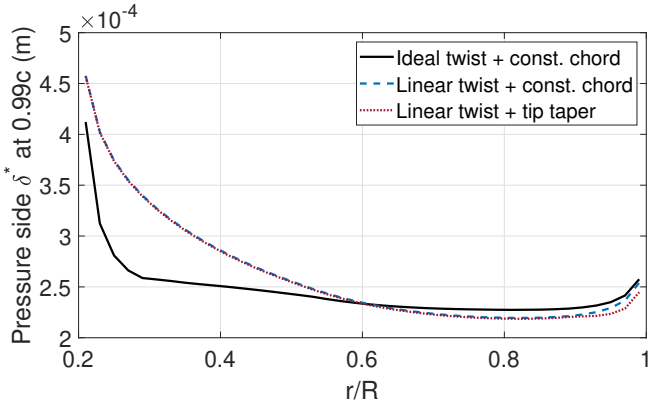

(b)

Fig. 13: Comparisons of the boundary layer displacement thickness at a 0.99 chord location for the blade ideal twist, linear twist, and taper on the rotor at a constant thrust for: (b) suction side, and (b) pressure side.

noise calculation in the BPM model requires an ad hoc adjustment of the Reynolds number limit, which is impractical without experimental data. Future efforts are needed to develop more robust LBL-VS noise predictions.

- The effect of leading-edge back-scattering is important when the reduced frequency (kc) is below 1.17, and this effect should be included for the broadband noise predictions on small-scale rotors.
- At the same thrust, the ideally twisted rotor is shown to have a slightly higher broadband noise level than the linearly twisted rotor. The tapered rotor blade tips can significantly reduce the broadband noise levels compared to the non-tapered blades.

ACKNOWLEDGEMENTS

The authors would like to acknowledge the support received as the recipient of the 2021 N&M Sarigul-Klijn Flight Research/Space Engineering award endowed on 17th December 2003 in commemoration of the 100th anniversary of powered flight with a purpose of encouraging students to conduct research in flight-related areas. The winning proposal title was "An Improved Method to Predict Small-scale Rotor Acoustics."

REFERENCES

[1]Colucci, F., "Unmanned Delivery Pending," Vertiflite Magazine, May/June, 2020.

[2]Air Force Research Laboratory Public Affairs, "Agility Prime announces 'flying car' military airworthiness, infrastructure milestones," 20 December, 2020.

[3]Floros, M., "Performance and Acoustics of Small Rotors with Non-Uniform Blade Spacing," Vertical Flight Society 75th Annual Forum, Philadelphia, Pennsylvania, May 13–16, 2019.

[4]Brentner, K., and Farassat, F., "Modeling Aerodynamically Generated Sound of Helicopter Rotors," *Progress in Aerospace Sciences*, Vol. 39 (2), 2003, pp. 83–120.

[5]Snider, R., Samuels, T., Goldman, B., and Brentner, K., "Full-Scale Rotorcraft Broadband Noise Prediction and Its Relevance to Civil Noise Certification Criteria," Proceedings of the 69th Annual Forum of the American Helicopter Society, Phoenix, AZ, May 21-23, 2013.

[6]Brentner, K., and Holland, P., "An Efficient and Robust Method for Computing Quadrupole Noise," *Journal of the American Helicopter Society*, Vol. 42 (2), 1997, pp. 172–181.

[7]Jia, Z., Lee, S., Sharma, K., and Brentner, K., "Aeroacoustic Analysis of a Lift-Offset Coaxial Rotor Using High-Fidelity CFD/CSD Loose Coupling Simulation," *Journal of the American Helicopter Society*, Vol. 65 (1), 2020, pp. 1–15.

[8]Jia, Z., and Lee, S., "Acoustic Analysis of a Quadrotor eVTOL Design via High-Fidelity Simulations," Proceedings of the 25th AIAA/CEAS Aeroacoustics Conference, Delft, The Netherlands, May 20-23, 2019.

[9]Jia, Z., and Lee, S., "Aeroacoustic Analysis of a Side-by-Side Hybrid VTOL Aircraft," Proceedings of the Vertical Flight Society 76th Annual Forum, Virtual Event, October 5-8, 2020.

[10]Sagaga, J., and Lee, S., "Acoustic Predictions for the Side-by-Side Air Taxi Rotor in Hover," Vertical Flight Society 77th Annual Forum, Virtual Event, May 11-13, 2021.

[11]Li, S., and Lee, S., "Prediction of Rotorcraft Broadband Trailing-Edge Noise and Parameter Sensitivity Study," *Journal of the American Helicopter Society*, Vol. 65 (4), 2020, pp. 1–14.

[12]Brooks, T., Marcolini, M., and Pope, D., "Main Rotor Broadband Noise Study in the DNW," *Journal of the American Helicopter Society*, Vol. 34 (2), 1989, pp. 3–12.

[13]Zawodny, N., Boyd, D., and Burley, C., "Acoustic Characterization and Prediction of Representative, Small-Scale Rotary-Wing Unmanned Aircraft System Components," Proceedings of the 72nd Annual Forum of the American Helicopter Society, West Palm Beach, FL, May 17-19, 2016.

[14]Zawodny, N., and Boyd, D., "Investigation of Rotor-Airframe Interaction Noise Associated with Small-Scale Rotary-Wing Unmanned Aircraft Systems," *Journal of the American Helicopter Society*, Vol. 65 (1), 2020, pp. 1–17.

[15]Li, S., and Lee, S., "Acoustics Analysis of a Quiet Helicopter for Air Taxi Operations," Vertical Flight Society 77th Annual Forum, Virtual Event, May 11-13, 2021.

[16]Pettingill, N., Zawodny, N., Thurman, C., and Lopes, L., "Acoustic and Performance Characteristics of an Ideally Twisted Rotor in Hover," 2021 AIAA SciTech Forum, VIRTUAL EVENT, 19–21 January 2021.

[17]Roger, M., and Moreau, S., "Back-Scattering Correction and Further Extensions of Amiet's Trailing-Edge Noise Model. Part 1: Theory," *Journal of Sound and Vibration*, Vol. 286, 2005, pp. 477 – 506.

[18]Lee, S., Ayton, L., Bertagnolio, F., Moreau, S., Chong, T. P., and Joseph, P., "Turbulent boundary layer trailing-edge noise: Theory, computation, experiment, and application," *Progress in Aerospace Sciences*, Vol. 126, 2021, p. 100737.

[19]Amiet, R., "Noise Due to Turbulent Flow Past a Trailing Edge," *Journal of Sound and Vibration*, Vol. 47 (3), 1976, pp. 387–393.

[20]Curle, N., "The Influence of Solid Boundaries upon Aero-Dynamic Sound," *Proceedings of the Royal Society*, Vol. A231, 1955, pp. 505–514.

[21]Landahl, M., *Unsteady Transonic Flows*, Pergamon Press, 1961.

[22]Moreau, S., and Roger, M., "Back-scattering correction and further extensions of Amiet's trailing-edge noise model. Part II: Application," *Journal of Sound and Vibration*, Vol. 323, 2009, pp. 397–425.

[23]Amiet, R., "Effect of the Incident Surface Pressure Field on Noise due to Turbulent Flow Past a Trailing Edge," *Journal of Sound and Vibration*, Vol. 57 (2), 1978, pp. 305–306.

[24]Wolf, W. R., and Lele, S. K., "Trailing-Edge Noise Predictions Using Compressible Large-Eddy Simulation and Acoustic Analogy," *AIAA Journal*, Vol. 50 (11), 2012, pp. 2423–2434.

[25]Howe, M., "Noise produced by a sawtooth trailing edge," *The Journal of the Acoustical Society of America*, Vol. 90 (1), 1991, pp. 482–487.

[26]Ayton, L. J., "Analytic Solution for Aerodynamic Noise Generated by Plates with Spanwise-Varying Trailing Edges," *Journal of Fluid Mechanics*, Vol. 849, 2018, p. 448–466.

[27]Lyu, B., and Ayton, L. J., "Rapid noise prediction models for serrated leading and trailing edges," *Journal of Sound and Vibration*, Vol. 469, 2020, p. 115136.

[28]Zarri, A., Christophe, J., Moreau, S., and Schram, C., "Influence of Swept Blades on Low-Order Acoustic Prediction for Axial Fans," *Acoustics*, Vol. 2 (4), 2020, pp. 812–832.

[29]Li, S., and Lee, S., "Prediction of Urban Air Mobility Multirotor VTOL Broadband Noise Using UCD-QuietFly," *Journal of the American Helicopter Society*, Vol. 66 (3), 2021, pp. 1–13.

[30]Thurman, C., Zawodny, N., Pettingill, N., Lopes, L., and Baeder, J., "Physics-Informed Broadband Noise Source Identification and Prediction of an Ideally Twisted Rotor," 2021 AIAA SciTech Forum, VIRTUAL EVENT, 19–21 January 2021.

[31]Casalino, D., Grande, E., Romani, G., Ragni, D., and Avallone, F., "Definition of a Benchmark for Low Reynolds Number Propeller Aeroacoustics," *Aerospace Science and Technology*, Vol. 113, 2021, p. 106707.

[32]Pettingill, N., and Zawodny, N., "Acoustic Characterization and Prediction of Representative, Small-Scale Rotary-Wing Unmanned Aircraft System Components," Proceedings of the Vertical Flight Society 75th Annual Forum & Technology Display, Philadelphia, PA, May 13–16, 2019.

[33]Lee, S., "Empirical Wall-Pressure Spectral Modeling for Zero and Adverse Pressure Gradient Flows," *AIAA Journal*, Vol. 56 (5), 2018, pp. 1818–1829.

[34]Thai, A. D., De Paola, E., Di Marco, A., Stoica, L. G., Camussi, R., Tron, R., and Grace, S. M., "Experimental and Computational Aeroacoustic Investigation of Small Rotor Interactions in Hover," *Applied Sciences*, Vol. 11 (21), 2021.

[35]Li, S., and Lee, S., "A Machine Learning-Based Fast Prediction of Rotorcraft Broadband Noise," Proceedings of the 2020 AIAA Aviation Forum, Virtual Event, June 15-19, 2020.

[36]Amiet, R., "Acoustic Radiation from an Airfoil in a Turbulent Stream," *Journal of Sound and Vibration*, Vol. 41 (4), 1975, pp. 407–420.

[37]Rozenberg, Y., Roger, M., and Moreau, S., "Rotating Blade Trailing-Edge Noise: Experimental Validation of Analytical Model," *AIAA Journal*, Vol. 48 (5), 2010, pp. 951–962.

[38]Brooks, T., Pope, D., and Marcolini, M., "Airfoil Self-noise and Prediction," , 1989. NASA RP 1218.

[39]Brooks, T., and Hodgson, T., "Trailing Edge Noise Prediction from Measured Surface Pressures," *Journal of Sound and Vibration*, Vol. 78 (1), 1981, pp. 69–117.

[40]Jung, Y., Baeder, J., and He, C., "Investigation of Empirical Rotor Broadband Prediction using CFD Boundary Layer Parameters Extraction," Vertical Flight Society 77th Annual Forum, Virtual Event, May 11-13, 2021.

[41]Johnson, W., "Technology Drivers in the Development of CAMRAD II," American Helicopter Society Aeromechanics Specialist Meeting, San Francisco, California, January 1994.

[42]Li, S., "Development of Rotorcraft Forward Flight Analysis Code Using the Finite-State Dynamic Inflow Model," Master's thesis, University of California Davis, August 2020.

[43]Peters, D., Boyd, D., and He, C., "Finite-State Induced-Flow Model for Rotors in Hover and Forward Flight," *Journal of the American Helicopter Society*, Vol. 34 (5), 1989, pp. 5–17.

[44]Johnson, W., *Helicopter Theory*, Dover Publication, 1994.